Journal of Materials Chemistry A

Accepted Manuscript

ROYAL SOCIETY OF CHEMISTRY

www.rsc.org/materialsA

Insight into the electrochemical behavior of micrometric Bi and Mg_3Bi_2 as performant negative electrodes for Mg batteries

Fabrizio Murgia, Lorenzo Stievano, Laure Monconduit and Romain Berthelot*

Institut Charles Gerhardt de Montpellier (UMR 5253 CNRS Unité de Montpellier)
Équipe Agrégats Interfaces Matériaux pour l'Énergie
2, Place Eugène Bataillon – CC1502 – 34095 Montpellier cedex 5 (France)
Réseau sur le Stockage Électrochimique de l'Énergie (FR 3459 CNRS)
33, Rue Saint Leu – 80039 Amiens cedex (France)

Abstract

The electrochemical behavior of micrometric Bi powder as active electrode material for Mg batteries is revisited in half-cell with Mg metal as counter electrode and organohaloaluminate-based complex electrolyte. A complete biphasic domain is evidenced from Bi to its Mg-alloyed counterpart Mg_3Bi_2. *Operando* X-ray diffraction underlines a simple mechanism that does not imply any intermediate phases or amorphization process. The high performances of Bi-based electrodes are confirmed using an optimized electrode formulation, with specific capacity nearing the theoretical value of 385 mAh/g at low rates. The capacity fading appears limited when moving to high current densities.

In parallel, micrometric Mg_3Bi_2 intermetallic compound obtained by high-energy ball-milling exhibits the similar electrochemical behavior. As a proof-of-concept as-prepared Mg_3Bi_2 is directly associated with Chevrel-type positive electrode and successfully tested as complete Mg-ion battery. Despite the high molar mass, the couple Bi/Mg_3Bi_2 can be considered as reliable negative electrode candidate and a reference system for testing the next generation of Mg-ion batteries electrolytes.

Corresponding author: Romain Berthelot: romain.berthelot@umontpellier.fr

Introduction

Since the early 90s the development and the continuous improvement of Lithium-ion batteries (LiBs) allowed a fast and unceasing diffusion of electronic portable devices.[1] Furthermore, LiBs start to be employed as stand-alone or tandem power sources for electric vehicle (EVs) and plug-in hybrid vehicles (PHVs), with the consequence of a near-term rising Li demand. However Li is a relatively rare and non-uniformly spread element on the earth crust and its possibility to be set as the ubiquitous component of energy storage devices is largely questioned.[2] Moreover, for application in the field of automotive transport, LiB technology has to face several not negligible safety issues, such as overheating and explosions.[3] In addition, despite years of huge improvements, LiB technology seems to near its limits in terms of energy density.[4] For all these reasons, exploring cheaper, safer and more performant alternative solutions to LiB systems is essential. Among them, a particular attention has been recently given to magnesium-based batteries (MBs).[5, 6, 7, 8, 9] Mg is the fifth most abundant element and is evenly spread element on the earth crust. It is not toxic, with a melting point of 650°C and is far less air-sensitive than Li, resulting more economically attractive and safer. Furthermore, Mg has a bivalent cation, is denser than Li and consequently capable to provide high volumetric energy density (3837 $mAh \cdot cm^{-3}$), which is approximately twice as high as Li metal and five times higher than graphite in LiBs.

In spite of these interesting features, the realization of a Mg-based battery is not a trivial task: preliminary studies about the deposition/stripping of Mg metal from usual electrolytes (Mg salt(s) dissolved in organic solvents) demonstrate an irreversible formation of a passivation layer on the electrode surface. This layer prevents the electrochemical deposition/stripping of Mg and consequently hinders any Mg-battery cycling investigations.[10, 11] Nevertheless, this issue was overcome by using ethereal solutions of Grignard reagents.[12, 13] These studies led to the pioneering work of Aurbach and coworkers that shows the feasibility of

rechargeable MBs, using Mg-organohaloaluminate complex electrolyte and proposing Chevrel-type molybdenum sulfide (Mo_3S_4) as the positive electrode.[14] Their tests reveal a high reversible formation of the Mg-intercalated phase $Mg_xMo_3S_4$, reaching a maximal charge capacity of 122 mA h g^{-1} at constant current density of 0.3 mA cm^{-2}. This work is still paving the way for the research of more efficient MBs; however, such electrolytes are very air-sensitive, corrosive with current collectors and suffers from anodic stability.[15, 16, 17] This latter represents a crucial drawback that hurdles the investigation on high-voltage positive electrode materials.[5, 9, 18] To date, there is no standard electrolyte that fills all the requirements for practical applications, preventing at present the development of commercial Mg-based systems.

In parallel with the development of better electrolytes,[19, 20, 21, 22] an alternative strategy is the replacement of Mg metal as the negative electrode in order to come back to conventional electrolytes.[6, 7, 8] In this direction, it was recently shown that some *p*-block elements are able to form reversible alloys with Mg at low potential.[23, 24, 25, 26] In particular, Bi forming the intermetallic compound Mg_3Bi_2, potentially delivers a specific theoretical capacity overcoming graphite in LiBs (385 *vs.* 372 mA h g^{-1}). The electrochemical activity of Bi *vs.* Li has been already briefly reported in literature.[27, 28] Its use as negative electrode for MiBs was firstly proposed by Arthur *et al.* on electrodeposited electrodes.[23] Bi showed reversible electrochemical alloying/de-alloying to Mg metal even at relatively fast C-rates but with a noticeable loss of capacity. The compatibility of Bi anodes with conventional Mg-ion electrolytes was also evidenced. In order to improve the performance of Bi-based anodes, Shao *et al.* proposed the use of Bi nanotubes (Bi-NT). [29] The nanometric size and the specific morphology of Bi-NT improve the kinetics of Mg ions diffusion into the electrode, and were suggested to prevent large expansion/shrinkage phenomena. Therefore,

such nanostructured electrodes exhibit performances in terms of specific capacity and coulombic efficiency. A complete Mg-ion battery was reported by associating an electrochemically pre-magnesiated Bi electrode with Mo_3S_4 as positive electrode. Despite these very interesting results, the techniques employed for the formulation of the Bi electrode are complicate and their industrial scale-up seems rather improbable. Moreover, although the proof of concept of reversible Mg alloying/de-alloying was given, to date there are no studies supporting the full explanation of the mechanism of the electrochemical reversible formation of the magnesiated phase Mg_3Bi_2.

In this work, the complete mechanism of the reversible alloying of Mg with Bi was revisited using various electrochemical techniques coupled to *operando* X-ray diffraction (XRD). Discarding nanostructuration strategies, simple electrode formulations were tested with micrometric Bi or Mg_3Bi_2 powders as active materials. As a preliminary study, the electrodes were analyzed as positive materials in half-cell battery with Mg metal as counter and reference electrode, with an Mg-organohaloaluminate complex-based electrolyte as electrolyte. A perfect biphasic domain was evidenced; either starting from Bi or Mg_3Bi_2, with especially no amorphization process and no intermediate phases in agreement with the phase diagram. The extremely high thermodynamical reversibility of the Bi/Mg_3Bi_2 system was also highlighted. Micrometric Bi-based electrodes were also tested under various current densities. A limited capacity fading was observed, and the performances reached the high values previously obtained with nanostructured materials. [29] Finally, ball-milled as-prepared Mg_3Bi_2 was directly implemented in a proof-of-concept Mg-ion battery *vs.* Chevrel phase Mo_3S_4 and successfully tested using a conventional electrolyte. These results confirm the interest of Bi or Mg_3Bi_2 as references systems for negative electrodes for Mg-based systems.

Experimental section

Electrochemical active materials were Bi or Mg_3Bi_2 micrometric powders. Commercial Bi chunks (99.999%, Fluka) were mechanically pulverized in Ar atmosphere for 10 minutes using a 3D-rotation Spex Mix/Miller 8000. The intermetallic compound Mg_3Bi_2 was prepared by mixing Mg (98%, Sigma-Aldrich, reagent, grade, 20-230 mesh) and as-milled Bi powder in the 3.3:2 molar ratio. The ball/powder mass ratio was 12:1. Mechanochemical synthesis was carried out with a total active milling time of 300 minutes. A 10% Mg in weight excess is needed to balance the Mg deposition during the ball-milling process.[30] Indeed, without this nominal excess, Bi residue peaks are still visible by XRD analysis.

For electrode formulation, both Bi and Mg_3Bi_2 powders were mixed with 25 wt.% of carbon black (CB, Saft, Y50A) and 5 wt.% of poly-tetrafluoroethylene (PTFE, DuPont, 6N) in an agate mortar and spread on a flat surface to form a single auto-supported film. Disks were cut out of the film and stored in an argon-filled glove box in order to avoid any moisture contamination. The final mass of the active material is around 20-25 mg cm^{-2} (from one pellet to another). This formulation will be hereafter referred to as "self-supported electrode" and mainly used for the preliminary/low-current density tests and *operando* XRD analysis. Indeed such high loadings enable better resolution during XRD measurements. For rate-capability tests and cycling at high current density, optimized formulations were also prepared by mixing micrometric Bi with 9 wt.% of CB, 9 wt.% of vapor ground carbon fibers (VGCF, Showa Denko K.K., VGCF-H), 12 wt.% of polyvinilidenedifluorure (PVdF, Solvay, Solef 5130) and using N-methyl-2-pirrolydone (NMP, 99%, Sigma-Aldrich) as solvent. The so-obtained slurry was stirred in a planetary ball-mill for 1 hour, and subsequently casted onto a 100 µm Cu foil (99.9 %, Goodfellow), then dried at room temperature for 24 hours and finally 2 hours more in a vacuum flask at 80 °C. Disks of this film were cut out and stored in a glove

box. The final mass of the active material was precisely measured in glove box and found in the range 1-2 mg cm^{-2} (depending on the casted film). This formulation will be hereafter referenced as "Cu-foil supported electrode" and mainly used for the evaluation of the electrochemical performances. The morphology of both Bi and Mg_3Bi_2 raw powders, as well as films electrodes, was characterized by Scanning Electron Microscopy (SEM) using a Hitachi S-4800 microscope equipped with a field emission gun. Bi and Mg_3Bi_2 powders were stick upon a C-based conductive tape. Each sample was metallized for 15 seconds with a Pt source before the SEM analysis.

At this point, it is important to emphasize that the current study mainly focuses on investigating the electrochemical mechanism lying between Bi and Mg_3Bi_2. Therefore electrochemical tests were far from optimized rechargeable Mg-ion battery. Indeed both Bi and Mg_3Bi_2-based electrodes were electrochemically tested in a 2-electrode configuration Swagelok-type cell in which they were used as the positive working electrode, with a Mg disc (99.9%, Goodfellow) as both the reference and the negative counter electrode. Electrodes were electronically separated by 2 Whatman GF/A borosilicate glass fiber sheets. The choice of electrolyte was difficult. Keeping Mg metal as reference electrode involves the use of organohaloaluminate-based complex in ethereal solutions. Inspiring by the work of Singh *et al.* on electrodeposited Sn electrodes[24] a 1:1 mixture of EtMgCl (2.0M in THF, Sigma-Aldrich) and Et_2AlCl (97%, Sigma-Aldrich) was solubilized in anhydrous tetrahydrofuran (THF, ≥99.9% Sigma Aldrich).The final concentration of the $EtMg^{+}$-$Et_2AlCl_2^{-}$ complex formed *in situ* was estimated to be ~0.35 mol·L^{-1}. It is known that this electrolyte slightly suffers from limited performances (such as oxidation stability and coulombic efficiency) and more Mg-organohaloaluminate complex optimized formulations can be found in literature.[11, 31, 32, 33] However it is perfectly suitable for this current study mainly

focused on investigating the electrochemical mechanism. The complete Mg-ion battery was prepared in combining the as-prepared Mg_3Bi_2 with Mo_3S_4 Chevrel phase as positive electrode. The latter was synthetized following the recent protocol of Choi *et al.* [34] and briefly detailed in the supplementary information. A "conventional" electrolyte was prepared by solubilizing dry magnesium bis(trifluoromethanesulfonyl)imide ($Mg(TFSI)_2$, Solvionic, 99.5%) in diglyme (Sigma-Aldrich, 99.5%) in 0.5mol/L concentration.[35] All the necessary operations of cell assembly were carried out in glove-box. Electrochemical tests such as galvanostatic cycling with potential limitations (GCPL), cyclic voltammetry (CV) and galvanostatic intermittent titration technique (GITT) were performed using research-grade battery testers (BioLogic). Following the previous works devoted to the investigation of negative electrode materials using Mg-organohaloaluminate complex electrolytes [23, 24, 25, 26, 29], potential limitations were set to 0 and 0.8 V *vs.* Mg^{2+}/Mg. This electrochemical window enables one to avoid electrolyte decomposition [33] and perfectly suits the redox potential region of alloying and de-alloying plateaus of Bi. All these tests were performed at room temperature and repeated at least twice in order to verify the reproducibility of the results. C/*n* rate means that 1 mole of Mg reacts with 1 mole of active material in *n* hours. For structural characterization of both pristine and electrochemically formed phases, *ex situ* and *operando* analyses were performed with an Empyrean 2theta/omega diffractometer (PANalytical), equipped with the Cu Kα radiation. For *ex situ* measurements, the Swagelok-type cells were disassembled in the glove box, and the disk was washed with THF to remove any trace of electrolyte. In order to avoid oxidation reaction, all these measurements were performed protecting the samples with a Kapton tape. *Operando* measurements needed a specifically developed electrochemical cell, equipped with a Be window, described elsewhere.[36] In such a typical analysis, XRD pattern were collected every hour in the 20°–45° 2θ range, where most diffraction peaks of PTFE and Be are excluded. In this range,

however, there are enough peaks to clearly identify both Bi and Mg_3Bi_2 and to follow their evolution upon electrochemical cycling.

Results and discussion

1. *μ*-Bi *vs.* Mg

Figure 1 gathers the first 1.5 galvanostatic cycle obtained with a self-supported Bi electrode obtained from micrometric powder after chunks pulverization (Fig. S1), as well as an *ex situ* XRD collected at the end of discharge. During the first discharge, a single plateau occurs at 0.23 V, corresponding to the insertion of 1.53 mole of Mg into the Bi electrode likely through the alloying between Mg and Bi, according to the reaction[18]:

$$Bi + \frac{3}{2}Mg^{2+} + 3e^{-} \rightarrow \frac{1}{2}Mg_3Bi_2$$

This reaction is highly reversible: Mg de-insertion reaction occurs at 0.32 V during charge and the system shows a very limited polarization of about 90 mV. At the very beginning of the first discharge, the cell voltage drops rapidly down to ~0.11 V, but then rises again in a nonlinear fashion to finally reach the alloying plateau at 0.23 V. This feature was already observed in different systems [23, 24, 25, 26, 29] and illustrates the kinetic balance between the nucleation of Mg_3Bi_2 particles in the electrode and their subsequent growth. It is worth to note that Mg-Bi electrochemical alloying potential is extremely stable until achieving the theoretical capacity of 385 mA h g^{-1}. High capacity retention is shown after the first charge in which 95 % of first discharge capacity is observed (1.46 Mg is deinserted).

The *ex situ* XRD pattern of the electrode collected at the end of the first discharge confirms the quasi-complete magnesiation of the pristine electrode (Fig. 1.b). Indeed a highly

crystallized Mg_3Bi_2 phase is evidenced with refined cell parameters in complete agreement with the literature. [37] The second discharge shows almost the same behavior of the first one, with the exception of two remarkable differences. First, the plateau corresponding to Mg insertion is slightly higher in potential (0.26 V), and then this potential is reached more rapidly than in the first discharge, almost without the characteristic initial potential drop described above. Both effects can be explained by an unexplored electrolyte evolution or more likely assuming a morphology modification of the active material grains after the first discharge (known as the electrochemical grinding). Indeed, the electrochemical alloying reaction of Bi with Mg during the first discharge involves a size reduction (milling) of the micrometric Bi particles which requires high energy. In subsequent cycles the particles reactivity is therefore improved and less needed energy and leads to lower polarization for both alloying and de-alloying process. This effect is clearly underlined by cyclovoltammetry analysis where a potential shift is observable between the first and the second reduction (see inset of Fig. 1a). A weak potential variation is observed during the first charge around x = 0.5. This variation could be explained by assuming different electrochemical pathways for the two distinct Mg sites of Mg_3Bi_2 (the structure of Mg_3Bi_2 evidences two distinct Mg crystallographic sites with different coordination). However, this hypothesis seems unlikely based on the *in situ* XRD investigation presented below, and it is more consistently attributable to differences in grain size of the Mg_3Bi_2 particles formed during the first charge. Indeed the weak variation is not observed any more in the subsequent charge sequences.

In parallel with continuous galvanostatic tests, a GITT analysis was performed in order to better understand the mechanism of Mg insertion/de-insertion in Bi (Fig 2). In this chronoamperometric technique, a constant current flux is applied to the cell in order to insert/de-insert Mg ions for a determined period of time, followed by an open-circuit voltage (OCV) period, in which the battery relaxes and reaches a steady-state potential. This process

was repeated until the complete magnesiation/de-magnesiation was achieved. Following the close-circuit voltage (CCV) points, it is possible to find again the same trend shown in the GCPL in both discharge and charge. Nevertheless, looking to the OCV points, during the discharge an extremely stable thermodynamic potential is achieved at ~0.27 V and an almost identical value can be found on the subsequent charge, showing the very high reversibility of the Mg/Bi alloying reaction. Moreover, it is possible to confirm that the characteristic potential drop during the very first moments of the discharge should be ascribed to a kinetic effect because the OCV profile decreases directly down to the thermodynamic value without any oscillation (see inset in Fig. 2). It is also interesting to note that the difference between CCV and OCV in the plateau region is very small, and that the OCV potential is reached after an extremely fast relaxation (Fig. S2), evidencing a quasi-absence of kinetic limitation during the alloying reaction.

To verify this hypothesis and thoroughly investigate the structural changes involved in Mg/Bi alloying/de-alloying, an *operando* XRD study was performed upon an autosupported electrode cycled at C/20 (12.8 mA g^{-1}) over 1.5 cycles (Fig. 3). As soon as the first discharge progresses, the Bi diffraction peaks intensity decreases, while the Mg_3Bi_2 diffraction peaks simultaneously grow. This is also proved by the evolution curves of the integrated areas of the Bi (102) and Mg_3Bi_2 (102) selected diffraction peaks showing a perfect match between the maximum and minimum of each curve (Fig. 4). It is noticeable that no delay occurs in the observation of the biphasic process as usually reported in LiB due to the SEI formation. The reversible phenomenon is also observed during the following charge. Interestingly this biphasic transition happens without any amorphization process, as it was previously observed for other alloy-type negative electrode materials *vs.* Li and/or Na.[38] Profile matching refinements performed on all collected XRD patterns reveal that both Bi and Mg_3Bi_2 cell

parameters remain constant during the whole electrochemical cycling. This confirms that even at very low Mg insertion values, there is no Mg-solubility in the Bi matrix, in total agreement with the Bi-Mg phase diagram.[39] All the diffraction peaks of Mg_3Bi_2 evolve in the same trend either during discharge or charge process. This cannot allow differentiating two distinct electrochemical pathways for the two Mg sites.

2. *μ*-Mg_3Bi_2 *vs.* Mg

For MiB configuration a source of Mg ions is necessary either in the positive or in the negative electrode material. Bi-based electrodes should be therefore associated with Mg-containing positive electrode materials such as silicates ($MgMSiO_4$ [40, 41, 42]) or polyanionic compounds ($MgMPO_4F$ [43, 44]). It is also very important to investigate Mg-containing negative electrode materials in order to anticipate a possible next generation of Mg-free positive electrode materials. [45] For these reasons, the electrochemical behavior of as-prepared Mg_3Bi_2 was also investigated in this study. Micrometric Mg_3Bi_2 powder can be easily obtained in only 5 hours of milling, as evidenced by XRD (Fig. S3). The two first galvanostatic and CV cycling with Mg_3Bi_2-based electrodes are presented in Figure S4. Almost complete electrochemical Mg de-alloying reaction is obtained, with a highly reversible capacity (95% retention in the subsequent discharge). During the first charge, the de-alloying process occurs around 0.5 V. This polarization, once compared to the value observed on charge when starting from micrometric Bi electrodes, can be attributed to the higher energy needed for de-alloying micrometric particles of Mg_3Bi_2. In fact, after this electrochemical grinding, subsequent discharge and charge plateaus occur at the same potential than these observed for the micro-Bi based electrodes (Fig. 1). The charge/discharge process was also followed by *operando* XRD analysis. The biphasic mechanism is clearly

evidenced by the disappearance/appearance of the diffraction peaks of both Mg_3Bi_2 and Bi, as well as by their constant cell parameters (Fig. S5 and S6).

3. Performances evaluation

Besides exploring the electrochemical mechanism it is worth trying to compare the performances of electrodes based on micrometric powders as active materials with the observations of the literature. Indeed easily scale-up formulations would be preferred if further applications are considered. Cu-foil supported electrodes were tested at different current densities from C/100 to 2C (for consistency only cycling collected at 2C is presented). The initial potential local minimum observed at low rates is more pronounced with higher current density. Consequently, the cut-off value of 0 V *vs.* Mg^{2+}/Mg is sometimes directly reached and several short activation cycles are therefore necessary to overcome this potential drop and reach the alloying plateau. Figure 5 shows galvanostatic cycles at 2C (subsequent to a few activation sweeps) on a Cu-foil supported electrode, as well as a SEM picture illustrating the intimate mixing between active material (micrometric Bi) and additives (carbon and polymer binder). Here also the alloying and de-alloying process is clearly highlighted by the flat potential plateau. The battery exhibits a mean reversible capacity of about 300 mA h g^{-1}, only 22% lower than the theoretical one, with a slight but steady decrease, and a coulombic efficiency stabilized around 98.5% after 50 cycles. The alternating strong volume changes (~100%) during the alloying and de-alloying process might also contribute to the capacity fading with a progressive loss of electric contact between the active material grains and conductive additive. A continuous growing of SEI might be a possible explanation. In Mg battery, the SEI formation on negative electrode materials based on *p*-block elements remains a still completely unexplored domain. Surface characterization

techniques are in progress to better understand the electrode-electrolyte interface evolution in such systems.

The electrochemical performances of the micrometric Bi-based electrode were also evaluated through rate capability tests from C/20 to 5C (Fig. 6). Here again, a steady decrease of the capacity with increasing current density is observed. The performances are in line with those obtained with Bi-NT electrodes.[29] In addition, it is interesting to note that high capacities are obtained and remain constant for each C/20 cycling following a few cycles at high rates. In fact, the electrochemical grinding which progressively divides the pristine micrometric powder acts as an *in situ* self-nanostructuration. This process is responsible of the excellent electrochemical cycling properties of Bi *vs.* Mg, and questions the needs of starting from previously nanostructured electrode materials in the particular case of Bi.

4. Full Mg-ion cell: Mo_3S_4 vs. Mg_3Bi_2

In their previous work Shao *et al.* associated a pre-magnesiated Bi-NT with Chevrel phase Mo_3S_4 postive material for the first proof-of-concept of rechargeable Mg-ion battery with Bi-based electrode. [29]. At C/10, a reversible capacity of 60mAh/g was measured. However whithout any further details on the equilibration between the electrodes, it is rather difficult to analyse such results. In this present work, it was decided to intentionnaly set Mg_3Bi_2 as the limiting electrode (details in supporting information). The first cycling are presented in Figure 7. In a 2-electrode configuration the recorded potential directly reflects both electrodes evolution. In discharge the average value of 0.6 V matches with the Chevrel phase magnesiation potential (~1.1-1.2 V *vs.* Mg^{2+}/Mg, *cf.* Fig. S7) substracted by the first demagnesiation Mg_3Bi_2 plateau (0.5 V *vs.* Mg^{2+}/Mg, *cf.* Fig. S4). The process seems reversible and *ex situ* XRD validates the formation of Bi and $Mg_xMo_3S_4$. The slight potential oscillations at the end of discharge might express some intermittent contact losses. The global

shape of the discharge and charge greatly matches with what was previously observed on Mo_3S_4/Mg_3Bi_2 and Mo_3S_4/Mg_2Sn full cells.[24, 29] Unfortunately, a complete demagnesiation of Mg_3Bi_2 is not yet achieved. The relatively viscosity of diglyme compared to the Mg-organohaloaluminate electrolyte might hinder the electrochemical process and therefore limits the demagnesiation yield. This preliminary result is still encouraging and validates the strategy of investigating micrometric ball-milled Mg_3Bi_2 as viable Mg-containing negative electrode. However, challenges remain to optimize the full cell design and reach better overall performances.

Conclusions

The specific electrochemical behavior of Bi *vs.* Mg was briefly reported in the recent literature. In this paper, the complete mechanism was investigated using various electrochemical techniques coupled to *operando* X-ray diffraction. The biphasic process, between Bi and Mg_3Bi_2 occurs in the whole reaction range. This result is in agreement with the thermodynamic Bi-Mg phase diagram showing no Mg solubility in Bi and no additional compounds other than Mg_3Bi_2. While intermediate amorphization is usually observed in other alloy-type electrodes, in the special case of Bi and Mg_3Bi_2, both phases remain highly crystallized during both the charge and the discharge. Mechanochemically prepared Mg_3Bi_2 also exhibits interesting behavior *vs.* Mg and has been successfully tested in prototype complete Mg-ion cell with conventional electrolyte. This study confirms the interest of *p*-block elements in the design of next-generation of magnesium-based storage systems.

Acknowledgements

The authors want to thank for research funding “Cellule Energie CNRS” (Projet Exploratoire 2014 Alabama) and “Region Languedoc Roussillon” for F.M. scholarship funding. R.B. wants to acknowledge M.-L. Doublet (ICGM-CTMM) for fruitful discussions. F.M. and R.B thank D. Cot (Institut Européen des Membranes, Montpellier) for the collection of the SEM images.

References

[1] M. Armand, J.-M. Tarascon. *Nature*, 2008, **451**, 652-657.

[2] J.-M. Tarascon. *Nat. Chem.*, 2010, **2**, 510.

[3] S. M. Rezvanizaniani, Z. Liu, Y. Chen, J. Lee. *J. Power Sources*, 2014, **256**, 110-124.

[4] R. Van Noorden. *Nature*, 2014, **507**, 26-29.

[5] E. Levi, Y. Gofer, D. Aurbach. *Chem. Mater.*, 2010, **22**, 860-868.

[6] H. D. Yoo, I. Shterenberg, Y. Gofer, G. Gershinsky, N. Pour, D. Aurbach. *Energy Environ. Sci.*, 2013, **6**, 2265-2279.

[7] P. Saha, M. K. Datta, O. I. Velikokhatnyi, A. Manivannan, D. Alman, P. N. Kumta. *Prog. Mater. Sci.*, 2014, **66**, 1-86.

[8] R. Mohtadi, F. Mizuno. *Beilstein J. Nanotechnol.*, 2014, **5**, 1291-1311.

[9] J. Muldoon, C. B. Bucur, T. Gregory. *Chem. Rev.*, 2014, **114**, 11683-11720.

[10] P. Novak, R. Imhof, O. Haas. *Electrochim. Acta*, 1999, **45**, 351-367.

[11] D. Aurbach, I. Weissman, Y. Gofer, E. Levi. *Chem. Record*, 2003, **3**, 61-73.

[12] T. D. Gregory, R. J. Hoffman, R. C. Winterton. *J. Electrochem. Soc.*, 1990, **137**, 775-780.

[13] C. Liebenow, Z. Yang, P. Lobitz. *Electrochem. Commun.*, 2000, **2**, 641-645.

[14] D. Aurbach, K. Gamolsky, B. Markovsky, G. Salitra, Y. Gofer, U. Heider, R. Oesten, M. Schmidt. *J. Electrochem. Soc.*, 2000, **147**, 1322-1331.

[15] J. Muldoon, C. B. Bucur, A. G. Oliver, J. Zajicek, G. D. Allred, W. C. Boggess. *Energy Environ. Sci.*, 2013, **6**, 482-487.

[16] R. E. Doe, R. Han, J. Hwang, A. J. Gmitter, I. Shterenberg, H. D. Yoo, N. Pour, D. Aurbach. *Chem. Commun.*, 2014, **50**, 243-245.

[17] T. Liu, Y. Shao, G. Li, M. Gu, J. Hu, S. Xu, Z. Nie, X. Chen, C. Wang, J. Liu. *J. Mater. Chem. A*, 2014, **2**, 3430-3438.

[18] M. M. Huie, D. C. Bock, E. S. Takeuchi, A. C. Marschilok, K. J. Takeuchi. *Coord. Chem. Rev.*, 2015, **287**, 15-27.

[19] R. Mohtadi, M. Matsui, T. S. Arthur, S.-J. Hwang. *Angew. Chem. Int. Ed.*, 2012, **51**, 9780-9783.

[20] T. J. Carter, R. Mohtadi, T. S. Arthur, F. Mizuno, R. Zhang, S. Shirai, J. W. Kampf. *Angew. Chem. Int. Ed.*, 2014, **53**, 3173-3177.

[21] O. Tutusaus, R. Mohtadi. *ChemElectroChem*, 2015, **2**, 51-57.

[22] O. Tutusaus, R. Mohtadi, T. S. Arthur, F. Mizuno, E. G. Nelson, Y. V. Sevryugina. *Angew. Chem. Int. Ed.*, 2015, **54**, 7900-7904.

[23] T. S. Arthur, N. Singh, M. Matsui. *Electrochem. Commun.*, 2012, **16**, 103-106.

[24] N. Singh, T. S. Arthur, C. Ling, M. Matsui, F. Mizuno. *Chem. Commun.*, 2013, **49**, 149-151.

[25] R. A. DiLeo, Q. Zhang, A. C. Marschilok, K. J. Takeuchi, E. S. Takeuchi. *ECS Electrochem. Lett.*, 2015, **4**, A10-A14.

[26] K. Periyapperuma, T. T. Tran, M. Purcell, M. Obrovac. *Electrochim. Acta*, 2015, **165**, 162-165.

[27] O. Crosnier, T. Brousse, X. Devaux, P. Fragnaud, D. Schleich. *J. Power Sources*, 2001, **94**, 169-174.

[28] W. Xianming, T. Nishina, I. Uchida. *J. Power Sources*, 2002, **104**, 90-96.

[29] Y. Shao, M. Gu, X. Li, Z. Nie, P. Zuo, G. Li, T. Liu, J. Xiao, Y. Cheng, C. Wang, J.-G. Zhang, J. Liu. *Nano Lett.*, 2013, **14**, 255-260.

[30] H. Kim, G. Jeong, Y.-U. Kim, J.-H. Kim, C.-M. Park, H.-J. Sohn. *Chem. Soc. Rev.*, 2013, **42**, 9011-9034.

[31] D. Aurbach, Y. Gofer, Z. Lu, A. Schechter, O. Chusid, H. Gizbar, Y. Cohen, V. Ashkenazi, M. Moshkovich, R. Turgeman, E. Levi. *J. Power Sources*, 2001, **97-98**, 28-32.

[32] D. Aurbach, H. Gizbar, A. Schechter, O. Chusid, H. E. Gottlieb, Y. Gofer, I. Goldberg. *J. Electrochem. Soc.*, 2002, **149**, A115-A121.

[33] O. Mizrahi, N. Amir, E. Pollak, O. Chusid, V. Marks, H. Gottlieb, L. Larush, E. Zinigrad, D. Aurbach. *J. Electrochem. Soc.*, 2008, **155**, A103-A109.

[34] S.-H. Choi, J.-S. Kim, S.-G. Woo, W. Cho, S. Y. Choi, J. Choi, K.-T. Lee, M.-S. Park, Y.-J. Kim. *ACS Appl. Mater. Interfaces*, 2015, **7**, 7016-7024.

[35] S.-Y. Ha, Y.-W. Lee, S. W. Woo, B. Koo, J.-S. Kim, J. Cho, K. T. Lee, N.-S. Choi. *ACS Appl. Mater. Interfaces*, 2014, **6**, 4063-4073.

[36] J. B. Leriche, S. Hamelet, J. Shu, M. Morcrette, C. Masquelier, G. Ouvrard, M. Zerrouki, P. Soudan, S. Belin, E. Elkaïm, F. Baudelet. *J. Electrochem. Soc.*, 2010, **157**, A606-A610

[37] E. Zintl, E. Husemann. *Z. Phys. Chem.*, 1933, **21**, 138

[38] A. Darwiche, C. Marino, M. T. Sougrati, B. Fraisse, L. Stievano, L. Monconduit. *J. Am. Chem. Soc.*, 2012, **134**, 20805-20811.

[39] H. Okamoto. *J. Phase Equilibria*, 1991, **12**, 390.

[40] Y. NuLi, J. Yang, Y. Li, J. Wang. *Chem. Commun.*, 2010, **46**, 3794-3796.

[41] Y. NuLi, Y. Zheng, Y. Wang, J. Yang, J. Wang. *J. Mater. Chem.*, 2011, **21**, 12437-12443.

[42] Y. Orikasa, T. Masese, Y. Koyama, T. Mori, M. Hattori, K. Yamamoto, T. Okado, Z.-D. Huang, T. Minato, C. Tassel, J. Kim, Y. Kobayashi, T. Abe, H. Kageyama, Y. Uchimoto. *Sci. Rep.*, 2014, **4**, 5622.

[43] J. Wu, G. Gao, G. Wu, B. Liu, H. Yang, X. Zhou, J. Wang. *RSC Adv.*, 2014, **4**, 15014-15017.

[44] Z.-D. Huang, T. Masese, Y. Orikasa, T. Mori, T. Minato, C. Tassel, Y. Kobayashi, H. Kageyama, Y. Uchimoto. *J. Mater. Chem. A*, 2014, **2**, 11578-11582.

[45] R. Zhang, F. Mizuno. *Preparation of high energy-density electrode materials for rechargeable magnesium batteries*, US patent 20140322595 A1.

Figure captions

Figure 1: Galvanostatic curve of Bi/Mg battery obtained at C/100 with self-supported film from micrometric Bi powder. The alloying/de-alloying reaction is clearly evidenced by the potential plateau and the cyclovoltammetric curve (inset). The potential shift between the 1st and 2nd discharges due the electrochemical powder milling is highlighted by the red arrow. The vertical black arrow points out the slight potential rising during oxidation. The XRD pattern collected *ex situ* at the end of the discharge (bottom) shows the electrochemical formation of Mg_3Bi_2 (observed, calculated and difference profile respectively on black dots, red and blue lines; Bragg position on green vertical bars). The peak (*) corresponds to the most intense diffraction peak of PTFE.

Figure 2: GITT curve obtained from Bi/Mg battery, with 1 hour of reduction/oxidation at C/50, followed by 2 hours of relaxation at OCV.

Figure 3: *Operando* XRD characterization of the first discharge, charge and second discharge of Bi/Mg battery. The biphasic transition from Bi to Mg_3Bi_2 is shown here, without any amorphization process. Profile matching refinements performed on all XRD patterns evidence no cell parameters changes for both Bi and Mg_3Bi_2. Similar results are observed starting from Mg_3Bi_2-based electrode (see Supplementary Information, Figure S1)

Figure 4: Evolution of integrated areas of Bi (102) and Mg_3Bi_2 (102) diffraction peaks collected during the *operando* XRD characterization.

Figure 5: Top, SEM picture Cu-foil supported electrode showing the micrometric Bi particles embedded by carbon additives. Bottom, the galvanostatic curve obtained with such formulation at 2C (after initial activation sweeps). In inset, evolution of discharge and charge capacities as well as the coulombic efficiency.

Figure 6: rate-capability test from C/20 to 5C recorded with Cu-foil supported electrode from micrometric Bi powder. The performances are also compared with results obtained from Bi-NT. [29]

Figure 7: First cycling of Mg-ion cell prototype with both Mo_3S_4 as positive and as-prepared ball-milled Mg_3Bi_2 as negative electrodes. Electrolyte is $Mg(TFSI)_2$ in diglyme at 0.5mol/L.

Figure 1

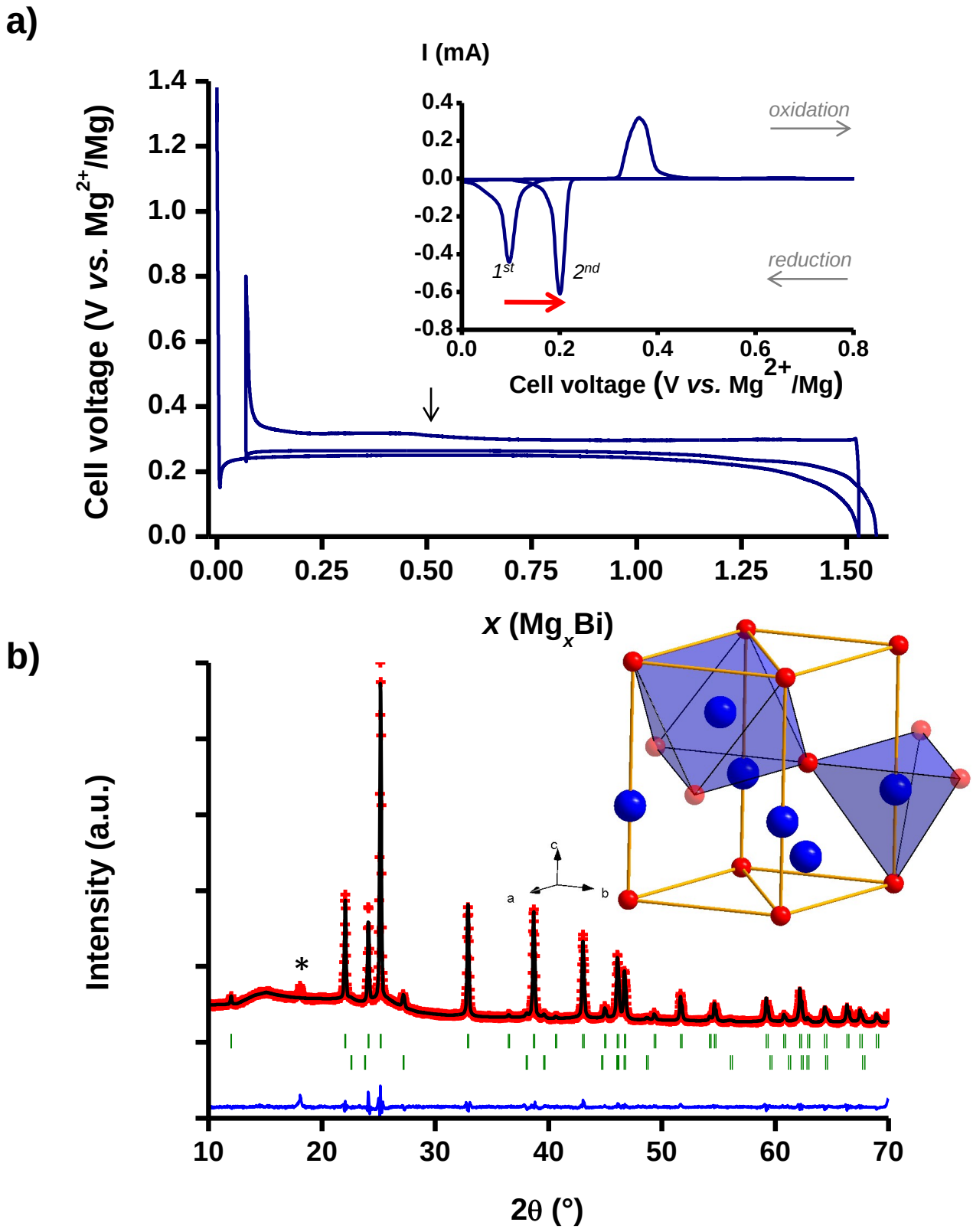

Figure 2

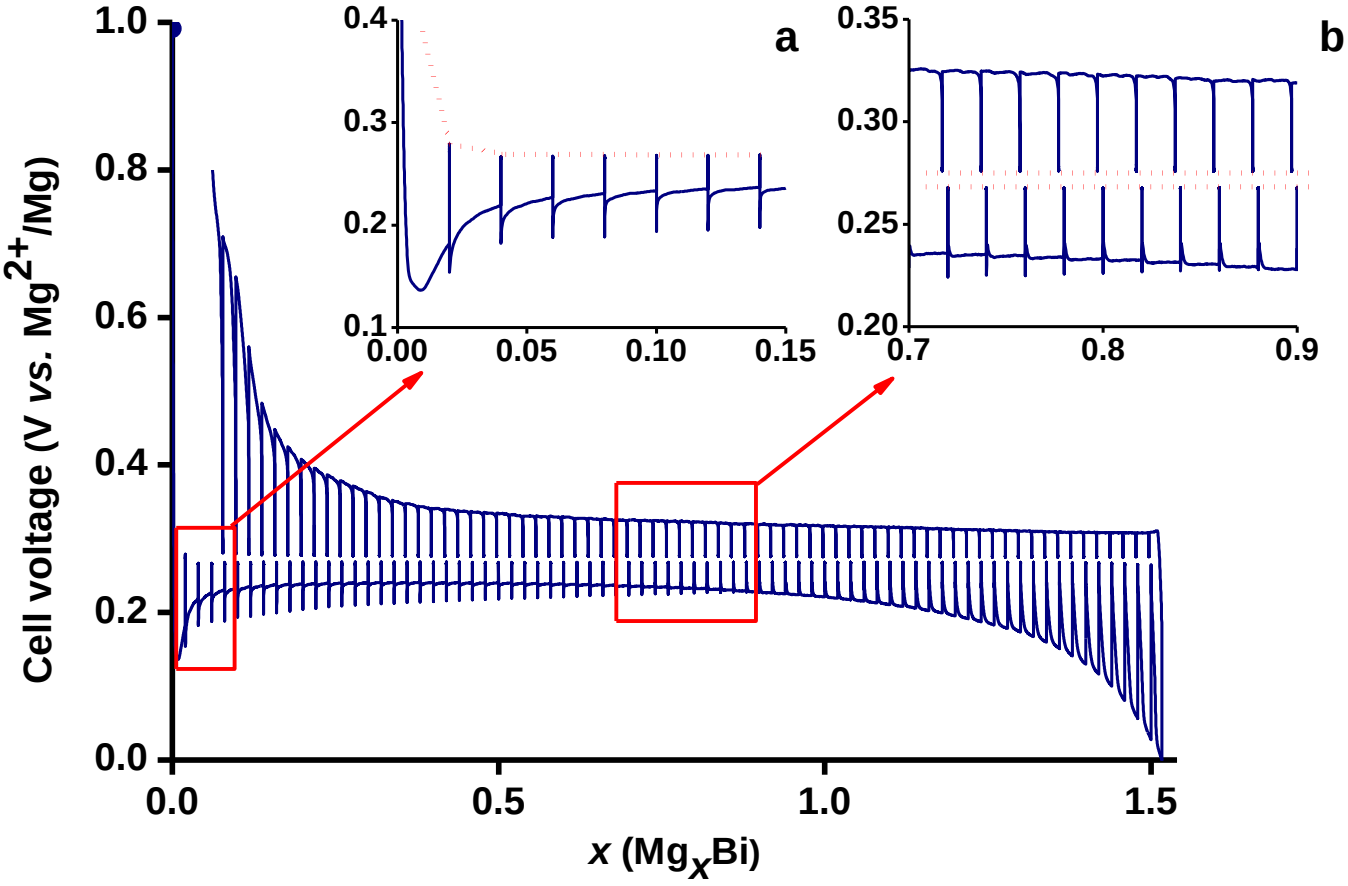

Figure 3

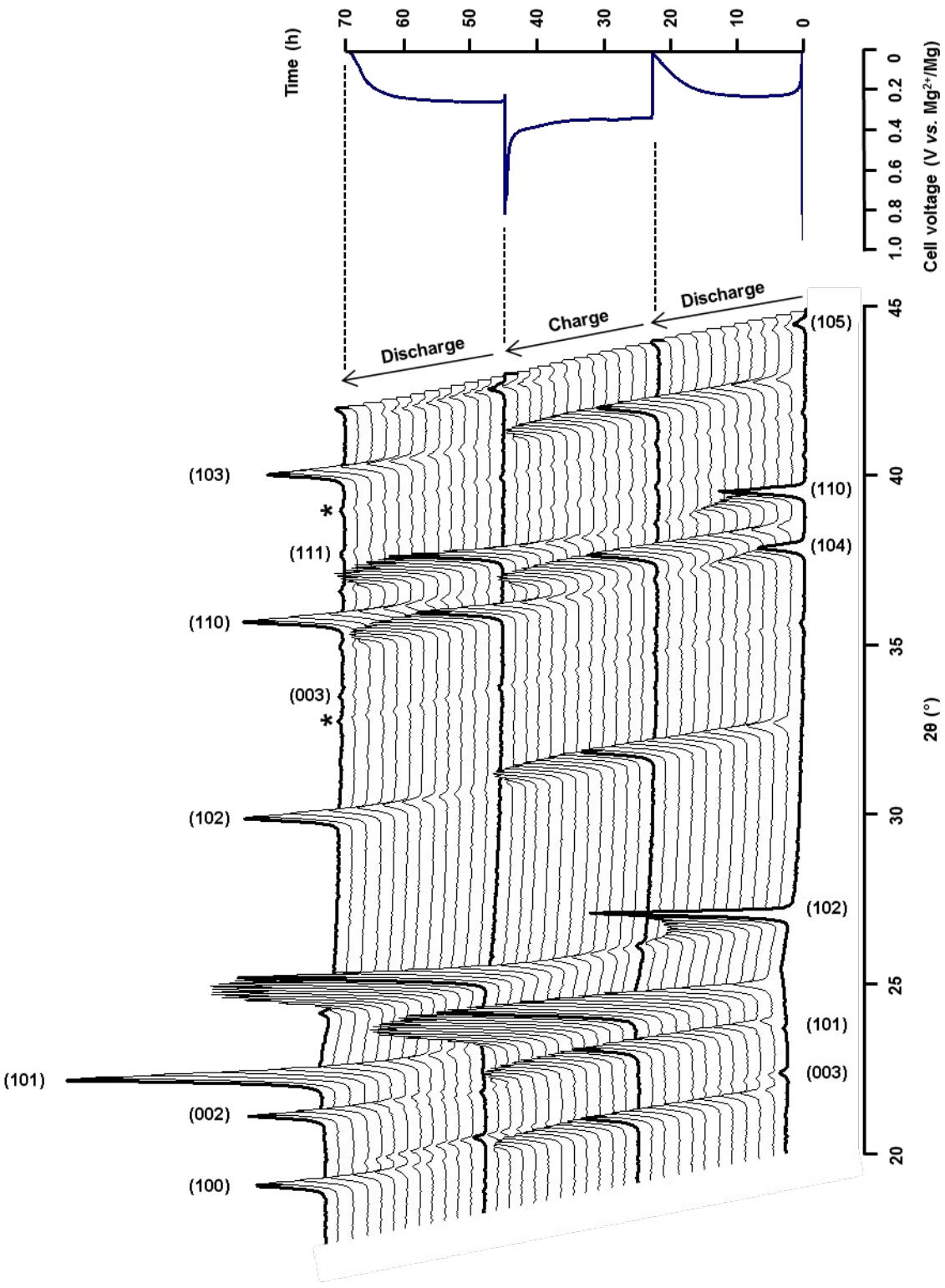

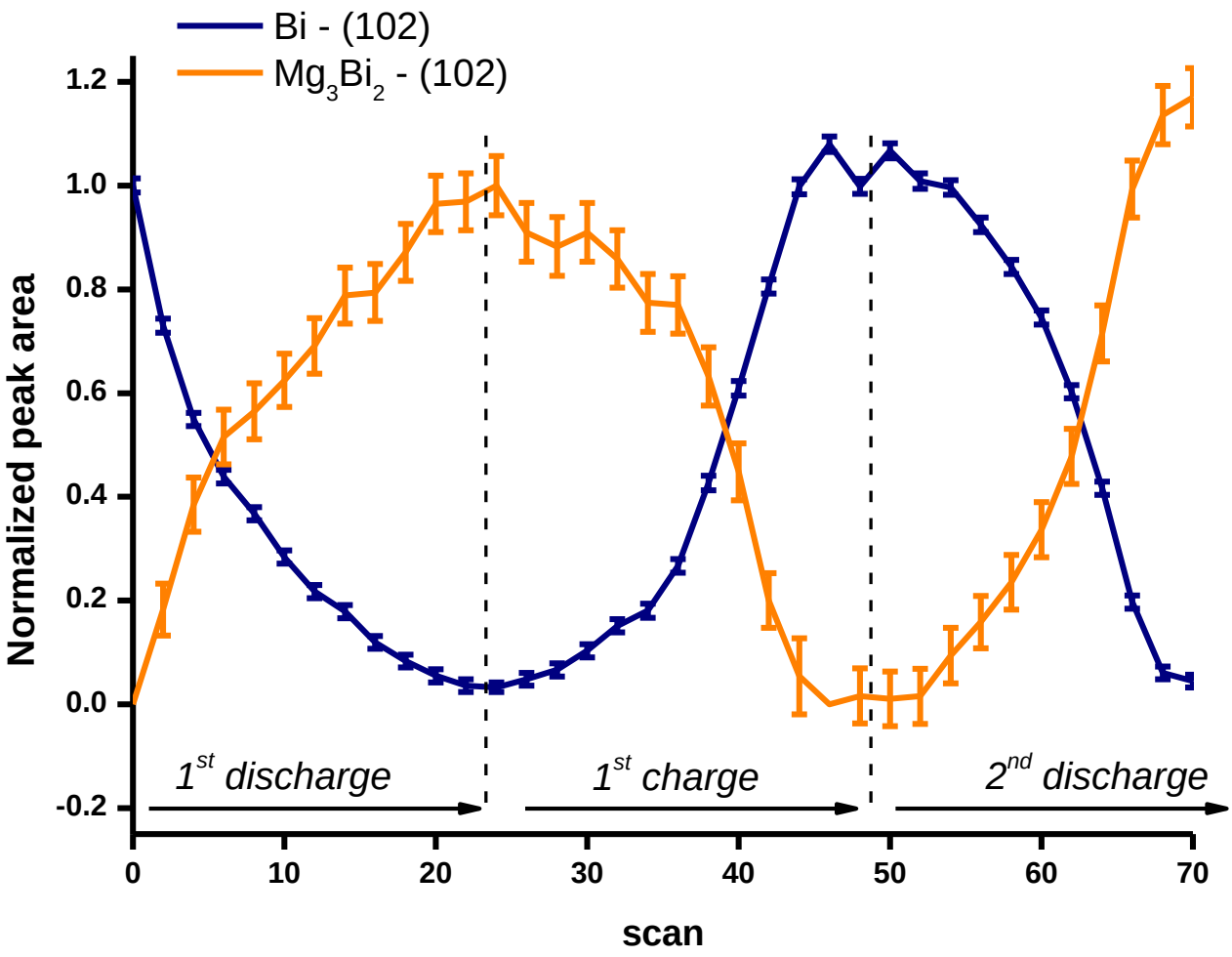

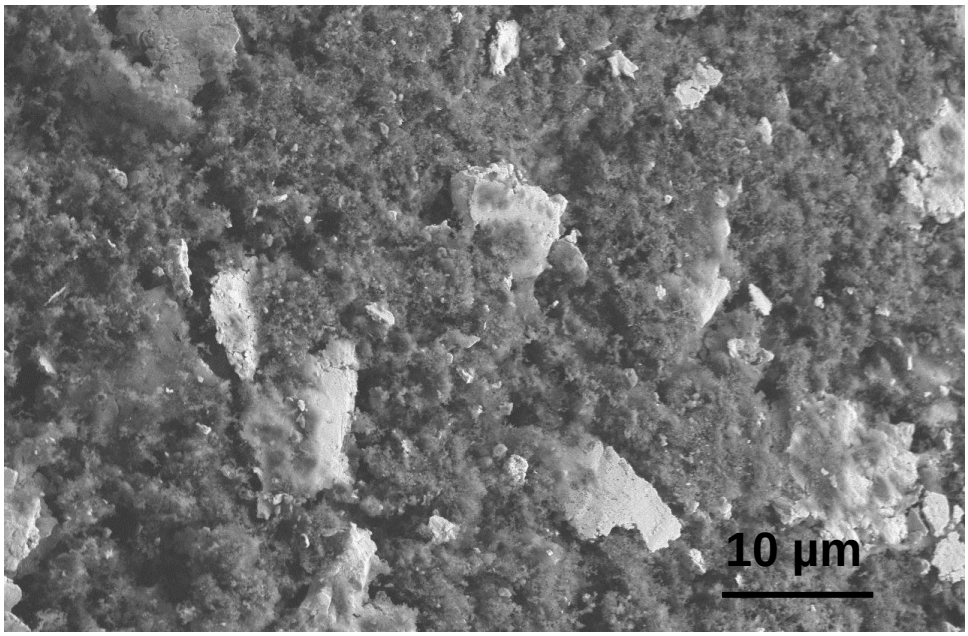

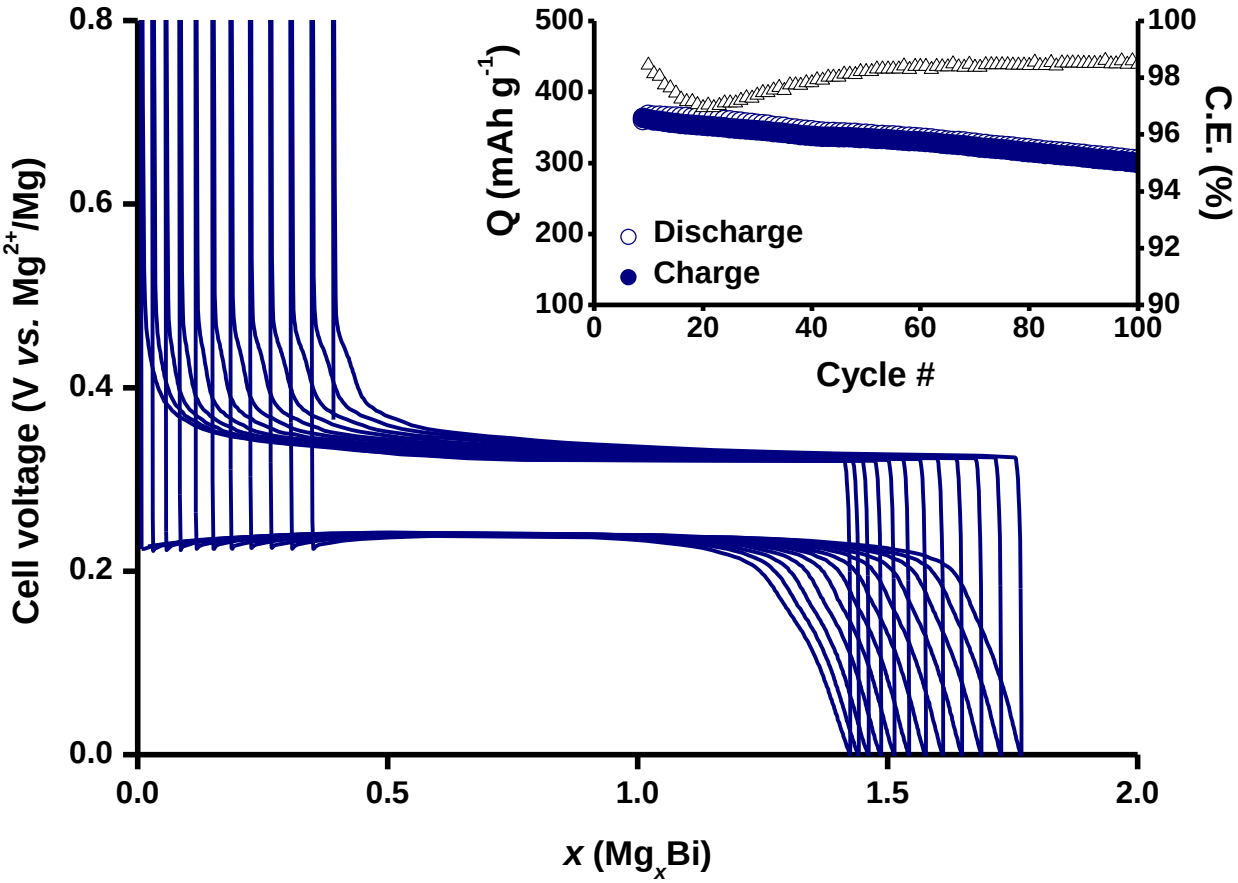

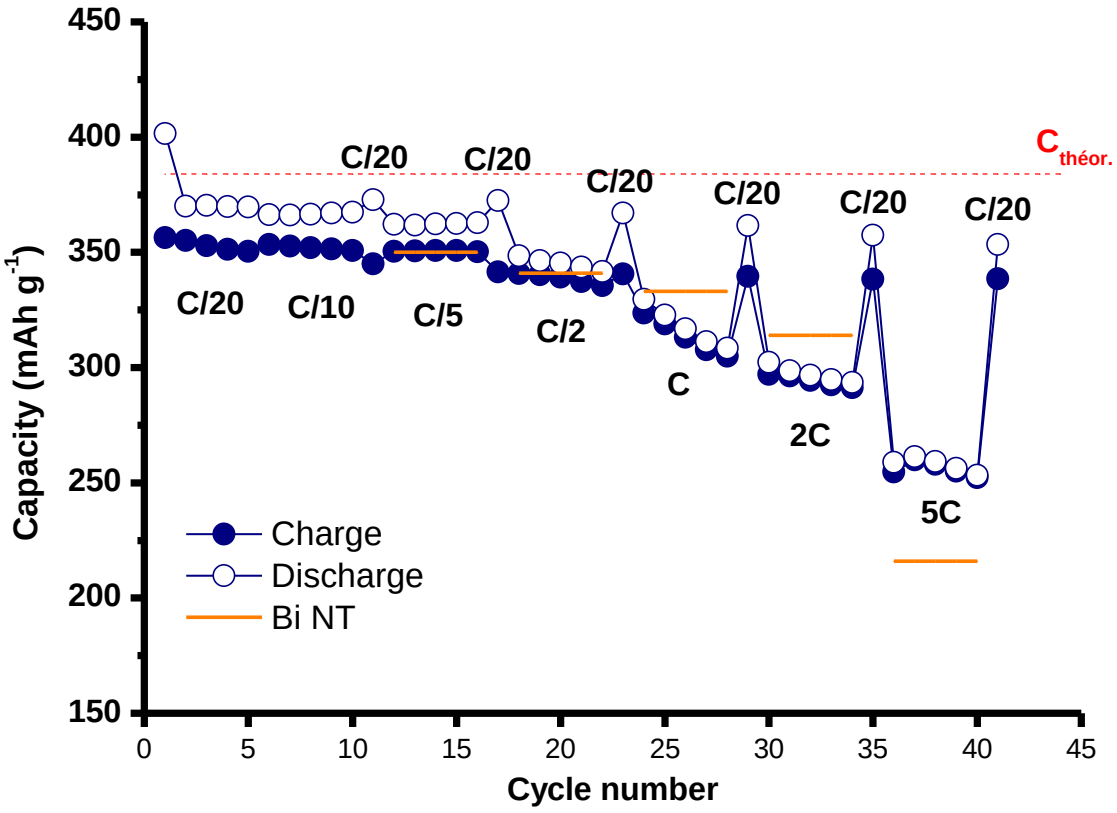

Figure 7

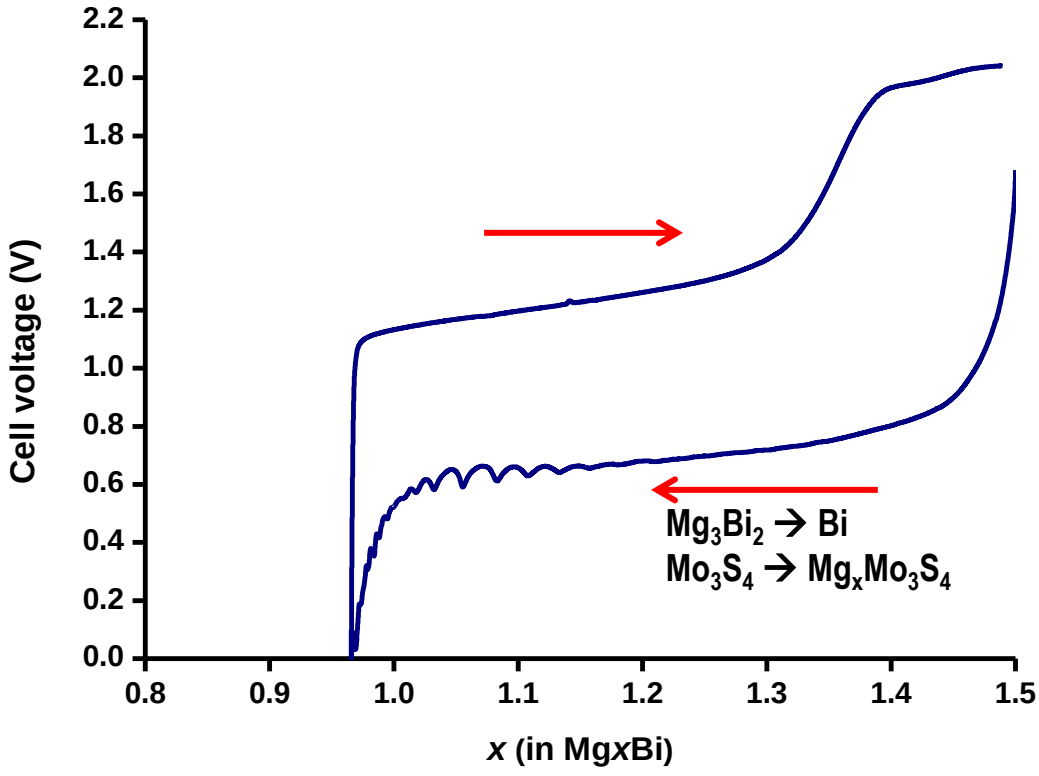

Table of content entry

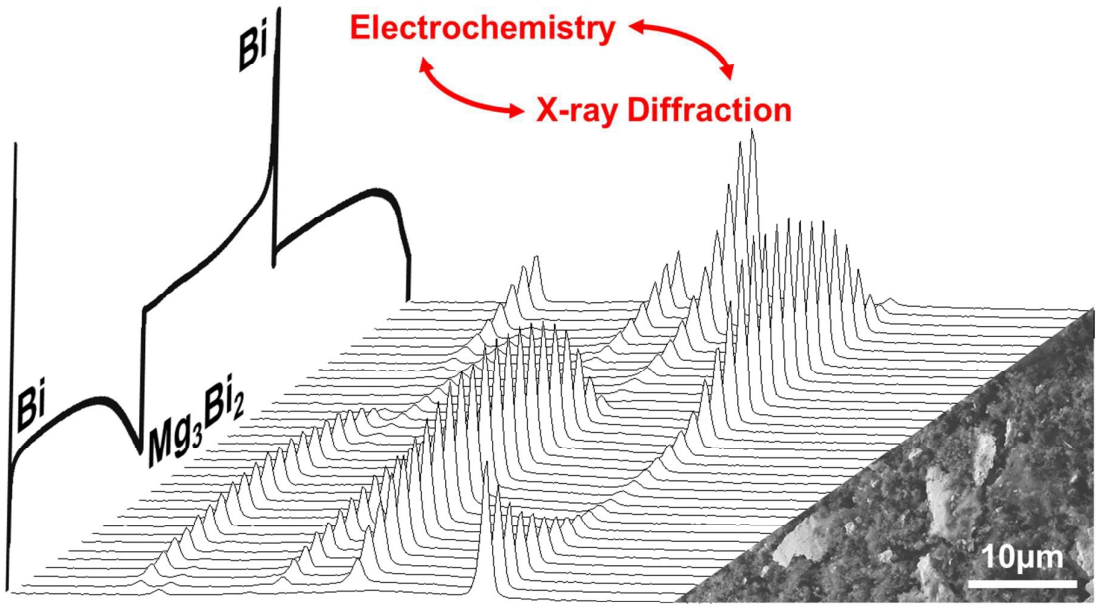

Bi & Mg_3Bi_2 : negative electrode materials for Mg-ion battery